

An Explainable 3D Residual Self-Attention Deep Neural Network For Joint Atrophy Localization and Alzheimer’s Disease Diagnosis using Structural MRI

Xin Zhang, Liangxiu Han, Wenyong Zhu, Liang Sun, Daoqiang Zhang

Abstract—Computer-aided early diagnosis of Alzheimer’s disease (AD) and its prodromal form mild cognitive impairment (MCI) based on structure Magnetic Resonance Imaging (sMRI) has provided a cost-effective and objective way for early prevention and treatment of disease progression, leading to improved patient care. In this work, we have proposed a novel computer-aided approach for early diagnosis of AD by introducing an explainable 3D Residual Attention Deep Neural Network (3D ResAttNet) for end-to-end learning from sMRI scans. Different from the existing approaches, the novelty of our approach is three-fold: 1) A Residual Self-Attention Deep Neural Network has been proposed to capture local, global and spatial information of MR images to improve diagnostic performance; 2) An explainable method using Gradient-based Localization Class Activation mapping (Grad-CAM) has been introduced to improve the interpretability of the proposed method; 3) This work has provided a full end-to-end learning solution for automated disease diagnosis. Our proposed 3D ResAttNet method has been evaluated on a large cohort of subjects from real datasets for two changing classification tasks (i.e. Alzheimer’s disease (AD) vs. Normal cohort (NC) and progressive MCI (pMCI) vs. stable MCI (sMCI)). The experimental results show that the proposed approach has a competitive advantage over the state-of-the-art models in terms of accuracy performance and generalizability. The explainable mechanism in our approach is able to identify and highlight the contribution of the important brain parts (e.g., hippocampus, lateral ventricle and most parts of the cortex) for transparent decisions.

Index Terms—Deep learning, 3D CNN, MRI brain scans, Model Explanation/Explainable Artificial Intelligence

I. INTRODUCTION

ALZHEIMER’S disease (AD) is the most common cause of dementia among the old people, which is irreversible and progressive neurodegenerative brain disease. It contributes to 60-70% of dementia cases and affects over 30 million individuals[1]. With the exponentially growing aging population across the globe, the prevalent increased cases of Alzheimer’s disease (AD) have presented unprecedented pressures on public healthcare service. There is currently no cure

Xin Zhang and Liangxiu Han are with the Department of Computing, and Mathematics, Manchester Metropolitan University, Manchester M15GD, U.K (e-mail: x.zhang@mmu.ac.uk; l.han@mmu.ac.uk)

Wenyong Zhu, Liang Sun, and Daoqiang Zhang are with the College of Computer Science and Technology, Nanjing University of Aeronautics and Astronautics, Nanjing 210016, China (e-mail: wyzhu@nuaa.edu.cn; sunl@nuaa.edu.cn; dqzhang@nuaa.edu.cn)

Corresponding authors: L. Han and D. Zhang (e-mail: l.han@mmu.ac.uk; dqzhang@nuaa.edu.cn)

for AD. However, the progress could be slowed through medicine and optimized physical cognition and activity. Therefore, accurate and timely diagnosis of Alzheimer’s disease (AD) and its early form mild cognitive impairment (MCI) is essential for optimal management and improved patient care [2]. Clinically, Structural Magnetic Resonance Imaging (sMRI) has been used for AD diagnosis. The structural MRI measurement is considered as a marker of AD progression, which can help detect the structural abnormalities and track the evolution of brain atrophy[3], [4], [5]. However, the disease identification process is mainly performed manually by specialists, which is time-consuming and expensive.

To solve this problem, much effort has been devoted to developing computer-aided diagnostic systems for automated discrimination of progression of AD (e.g., mild cognitive impairment (MCI) including progressive MCI (pMCI) and stable MCI (sMCI) and normal cohort (NC)) from sMRI scans based on voxel-wise global features, or predetermined regional features or combination of both [6], [7], [8], [9]. The volumetric or voxel-based approaches extract global features for detecting the structure changes and identifying voxel-wise disease associated microstructures for AD diagnosis [10], [11], [12], [13]. The Tensor-based morphology (TBM) diagnostic approach is a voxel-wise optimization approach, which can recognize local structural changes through mapping orders of local tissue volume loss or income over time to understand the neurodegenerative or neurodevelopment processes for AD diagnosis[14]. In [15], the gray matter voxels were selected as features and used to trained a machine learning model for AD vs. NC classification.

Since some specific brain regions such as hippocampal region of interest (ROI) are strongly correlated to the disease, several existing works focused on some predetermined ROIs guided by prior biological knowledge and extracted regional features for AD diagnosis [16], [17], [18], [19], [20]. For instance, Magnin [17] and Zhang [21] applied Support Vector Machine (SVM) to learn regional features for AD diagnosis by splitting the brain into some non-overlapping areas.

Recently, deep neural networks have shown successful for various computer vision tasks [22], [23]. A few deep learning methods have been proposed for AD diagnosis with sMRI scans and achieved better performance than the classical machine learning-based methods. These methods focused on learning either regional features from prior Knowledge regions

(e.g., hippocampus [24], [19], cortical [25]), global features [7] or combination of both [26]). Lian et al. proposed a hybrid deep learning approach using convolutional neural networks (CNNs) to learn combined features at multiscale [26]. Hosseini-Asl et al. predicted AD with a 3D CNNs based on the pretrained 3D convolutional autoencoder model to capture anatomical shape variations from sMRI [7].

Despite the existing encouraging work, it suffers several limitations. Firstly, extracting global features using voxel-based approaches involve processing high-dimensional 3D data, which is computationally intensive. Secondly, regional-based features focusing on certain brain regions of interest (e.g., the cortical thickness and hippocampus shape) may neglect possible pathological locations in the brain and fail to obtain global structural information for accurate AD diagnosis. Moreover, these methods require domain-specific prior-knowledge and multi-stage training. Thus, it is hard to provide an end-to-end solution for automatic disease diagnosis. Thirdly, the existing methods [26], [7] used combined features or global features to improve disease diagnostic performance based on deep learning approaches. However, the use of hybrid loss functions for each layer with the same shared weight may lead to difficulty in training and reproduction. Finally, most of existing deep learning-based approaches for AD diagnosis lack transparency in terms of model explanation due to the nature of black-box learning.

To overcome the aforementioned limitations, this work proposes a novel computer-aided approach for early diagnosis of AD from sMRI by developing an explainable 3D Residual Attention Deep Neural Network (3D ResAttNet) for end-to-end learning from sMRI. Different from the existing approaches, our contributions lie in:

- 1) A Residual Attention Deep Neural Network has been designed and implemented, allowing for capturing local, global and spatial information to improve diagnostic performance;
- 2) An explainable Gradient-based Localization Class Activation mapping (Grad-CAM) has been introduced, enabling visual explanation and interpretation of model predictions;
- 3) The proposed work has provided a full end-to-end solution for automated disease diagnosis.

The rest of this paper is organized as follows: Section 2 presents related work; Section 3 details the proposed method; In Section 4, the experimental evaluation is described; Section 5 concludes the proposed work and highlights the future work.

II. RELATED WORK

A. Computer-aided AD diagnosis

Computer-aided diagnosis of AD treatment has a long history, with the aim of extracting useful features for automatic classification. According to the feature extracted method, it can be broadly divided into three categories: 1) Global feature-based approaches (Voxel-based approaches); 2) Regional feature-based approaches; 3) Combination of both global and regional based approaches.

The early works on AD diagnosis mainly focused on the extracted global features from the whole MR image. The volumetric-based approach using voxel intensity features has been widely used for AD classification. Ashburner et al. [12] introduced a voxel-based morphometry (VBM) method, which used voxel-wise comparison on the smoothed gray-matter images. It showed the difference between white and gray voxels in local concentrations compared with the normal cohort (NC) brains. Based on the voxel-wise features, Klöppel et al. trained a support vector machine (SVM) model to diagnosis AD from sMRI [15]. Hinrichs et al. [27] also employed the gray-matter density to extract voxel-wise features, then a linear programming boosting method was trained to classify AD with sMRI images. However, some limitations include 1) computationally intensive and over-fitting due to high dimensionality of features with the relatively small number of images for model training; 2) neglecting the regional information that has been proven important to AD diagnosis.

The second category is regional feature-based methods. The majority of the works in this category mainly relied on prior knowledge to determine ROIs. Several existing works in the literature extracted features from the predetermined ROIs based on biological prior knowledge on the shrinkage of cerebral cortices and hippocampi, the enlargement of ventricles, and the change of regional glucose uptake [18], [19], [20]. Magnin [17] and Zhang [21] extracted regional features by splitting the whole brain into smaller regions to train the machine learning classifiers for AD diagnosis. The work in [16] used Gauss-Laguerre Harmonic Functions (GL-CHFs) and SURF [28] descriptors to extract local features from sMRI scans in hippocampus and posterior cingulate cortex (PCC) structures of the brain. Fan [29] partitioned the sMRI images into an adaptive set of brain areas based on the watershed algorithm, and then extracted the regional volumetric features to train a SVM-based AD classification model. However, these aforementioned methods are based on empirical regions, which might neglect possible pathological locations in the whole brain. Moreover, the features extracted from ROIs may not be able to reflect the subtle changes involved in the brain [30].

In order to address these limitations, a hierarchical method was introduced by combination of global and regional features. Lian et al. divided sMRI images into small 3D patches and extracted features, and then combined the features hierarchically [26]. Suk et al. also proposed a systematic method for a joint feature representation from the paired patches of sMRI images using the patch-based approach[30]. These patch-based methods have been proven to efficiently deal with the problem of high dimensional features and also the sensitivity to slight changes. However, these models always require multi-stage training, which are not an end-to-end solution.

Recently, deep learning has achieved a remarkable success in the field of Computer Vision, which has also become a popular and useful method for medical image analysis including Alzheimer's disease (AD) diagnosis based on MRI images. The convolutional neural network (CNN) [31] [32] has been proven to be suitable for grid-like data such as RGB images and MRI images. Billones et al. proposed a modified 16-layered VGG network to AD classification with

sMRI images [25]. The method selected 20 central slices of a sMRI image and achieved high accuracy on classification tasks using 900 sMRI images from the ADNI database. Residual network is the most widely used CNNs architecture that won the Imagenet classification competition [22]. It aims to alleviate the issues with the vanishing/exploding gradients when the network becomes deeper. In ResNet Block, a shortcut connection is added to link the input with the output, thus the Resnet learns the residual of input. Li et al.[33] proposed a deep network with residual blocks for AD diagnosis using 1776 sMRI images from the ADNI database.

B. Explainable deep learning

Due to the nature of black box, one challenge facing in the deep learning models is their explainable capability [34]. For the AD diagnosis task, most of existing deep learning-based approaches lack transparency with difficulty in explaining why and how a model decision is reached. To explain the image classification result by CNNs models, several explainable methods for CNNs have recently been proposed.

Saliency map [32] was firstly used for interpreting CNNs based models, which can highlight and explain which part of image features that contribute the most to the activity of a specific layer in a network or the decision of the network as a whole. It computes the gradients of logits based on the back-propagation algorithm and visualizes the feature contributions based on the amount of gradient they receive. This Saliency map is suitable for visualization but not good for localization and segmentation due to the noisy results [35]. Some improved methods based on saliency map [36], [37] have been proposed. For instance, the most widely used method is the guided backpropagation by preventing the backward flow of negative gradients on ReLU activation from the higher layer in the CNNs architecture [38]. Other optimized visualization methods also include PatternNet and PatternAttribution [39], Layer-Wise Relevance Propagation (LRP) [40] and DeepTaylor [41].

Class Activation mapping (CAM) is another explainable method for CNNs. In the CAM method, the top fully connected layers was replaced by convolutional layer to maintain the object positions and can find the spatial distribution of distinguished regions for predict category [42].

The CAM requires retraining the model since it changes the model architecture. However, to address this issue, Grad-CAM has been proposed as a generalization of the CAM method [43], which keeps the origin classification architecture and calculates the weight by pooling the gradient. This method has been widely used to explain the CNN classification models. However, since the Grad-CAM extracts the spatial distribution from the last layer of the feature map with low resolution, this results in smaller size than the input image size. In order to obtain more accurate location information at high resolution, some optimized CAM methods are proposed, such as Adversarial Complementary Learning for Weakly Supervised Object Localization (ACOL) [44], Self-produced Guidance for Weakly-supervised Object Localization (SPG) [45] and guided attention inference networks (GAIN) [46]. To the best of our knowledge, only a few works presented the explainable methods

for deep learning based AD Diagnosis. Montavon et al. and Yange et al. [41], [47] tried to explain 3D-CNNs by using visual interpretation methods. These methods are able to show how the CNNs made the classification decision. But there is no attempt made yet to explain 3D data classification tasks for diagnosis of MCI.

III. METHOD

The aim of this work is to develop an end-to-end deep learning framework to automatically classify discriminative atrophy localization on sMRI image for AD diagnosis, which consists of two levels of classifications: Alzheimer's disease (AD) vs. Normal cohort (NC) and progressive MCI (pMCI) vs. stable MCI (sMCI).

A. 3D Explainable Residual Self-Attention Convolutional Neural Network (3D ResAttNet)

We have proposed a 3D explainable residual attention network (3D ResAttNet), a deep convolutional neural network that adopts self-attention residual mechanism and explainable gradient-based localization class activation mapping (Grad-CAM) for AD diagnosis. The high-level conceptual framework is shown in Fig. 1, which consists of several major building blocks including 3D Conv block, Residual Self-attention block, and Explainable blocks. The rationale behind of this architecture design includes:

- 1) The residual mechanism is designed to allow for more efficient training with fewer parameters for performance enhancement when increasing the depth of the network. Existing methods [22] have shown that residual learning can alleviate the issue of disappearance/exploding gradients when the network becomes deeper. In addition, the residual connection avoids losing global features to ensure the integrity of the original information [48].
- 2) The self-attention mechanism is added to learn long-range dependencies. Capturing long-range dependencies is important in deep learning. Since the convolutional operator has a local receptive field, the long-distance dependencies can only be captured when repeatedly applying convolutional operations [49], [50], [51], [52], resulting in computational inefficiency. Hence, it is necessary to add self-attention mechanism to address these issues.
- 3) The gradient-based localization class activation mapping (Grad-CAM) is introduced to provide visual explanations of predictions of Alzheimer's disease.

B. 3D CNNs

Deep convolutional neural networks provide an effective way to learn multi-level features with multi-layers of convolutional operations in an end-to-end fashion [23]. Essentially, the high-level features are obtained by composing low-level features and the levels of features can be enriched by the number of stacked layers (i.e. depth). We have used 3D CNNs. 3D convolutions apply a 3D filter to the dataset and the filter moves 3 directions x , y , z to calculate the low-level feature

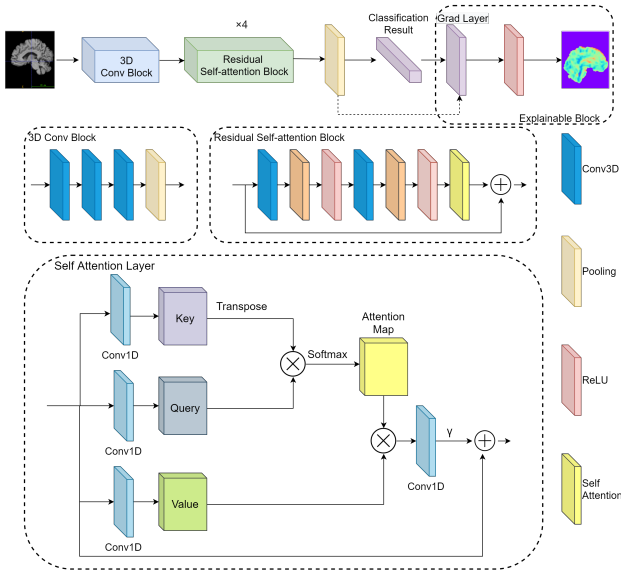


Fig. 1. The architecture of 3D residual attention deep Neural Network

representations of the output shape as a 3-dimensional volume space. The stack of three $3 \times 3 \times 3$ convolutional layer is used to improve computing efficiency, compared to the widely used $7 \times 7 \times 7$ convolutional layer.

C. Residual Self-attention block (ResAttNet)

In this work, for the first time, we have combined self-attention with residual module to capture both global and local information based on 3D images to avoid information loss. Attention mechanism has been a popular and useful tool in recent year [49], [50], which can learn and focus on the critical areas and suppress non-essential information through a weight matrix in whole image. On the other hand, this may cause global information loss. Therefore, we have added residual connection to address this issue. Residual network was originally designed to solve the issue of disappearance/exploding gradients when a network becomes deeper [22]. A residual connection is added between the origin input and the processed layer, which allows gradients to propagate more easily through the network.

1) Residual network layer:

A residual network can be formulated as follows:

$$y = x + r(x) \quad (1)$$

Where y is the output of the residual module, x is the input and $r(x)$ is the residual function. This module includes two Conv3D blocks consisting of $3 \times 3 \times 3$ 3D convolution layers, 3D batch normalization and rectified-linear-unit nonlinearity layer (ReLU).

2) Self-attention layer:

As described in Section III-A, the convolutional operator has a local receptive field and only performs local operations, while the self-attention mechanism can perform non-local operation, capable of capturing long-range dependencies/global information. Therefore, inspired by the work in [52], [51], in our work, the self-attention layer is introduced to the end

of original residual module $r(x)$ to help the model efficiently capture the global information. A self-attention function can be described as mapping a query, a key, and a value to the input, where those are all vectors. Key and value are the features of the whole sMRI extracted by each convolution block and the query determines which values to focus on for learning process. By using the $1 \times 1 \times 1$ convolution filter, the key, query, and value are transformed to vectors. The key, query and value are denoted by $f(x)$, $g(x)$, $h(x)$ as follows:

$$Key : f(x) = W_f x \quad (2)$$

$$Query : g(x) = W_g x \quad (3)$$

$$Value : h(x) = W_h x \quad (4)$$

Here $x \in R^{C \times N}$ is the features from the previous layer. C is the number of channels and N is the number of locations of features from the previous layer. W_f , W_g and W_h are all $1 \times 1 \times 1$ convolution filters. The self-attention map $(a_{i,j})$ can be calculated as:

$$a_{i,j} = \frac{\exp(f(x_i)^T g(x_j))}{\sum_{i=1}^n \exp(f(x_i)^T g(x_j))} \quad (5)$$

where $a_{i,j}$ indicates the correlative degree of attention between each region i and all other regions. j is the index of an output position. The output of the attention layer is $o = (o_1, o_1 \dots o_j, o_N) \in R^{C \times N}$, where

$$o_j = W_v \left(\sum_{i=1}^N a_{i,j} h(x_i) \right) \quad (6)$$

In order to keep the same number of channels as the original input and for memory efficiency, a $1 \times 1 \times 1$ convolution filter (W_v) is used to reduce the channel number of final outputs.

3) Residual Self-attention block (ResAttNet):

Therefore, the final output of the Residual Attention Block is given by:

$$y = x + r(x) + \gamma o(r(x)) \quad (7)$$

Where the $o(r(x))$ is the output of self-attention map, $r(x)$ is the output of original output of residual function and x is input feature, the γ is a learnable parameter. We set γ as 0 as default to allows the network to first rely on the cues in the local neighborhood. When γ increased, the model gradually learns to assign more weight to the non-local evidence.

D. The explainable 3D-CNNs

To understand inside the proposed deep model, the 3D Grad-CAM have been applied to explain the model decision.

We first calculated the gradient of the probabilities of disease areas with respect to the activation of unit k at location x, y, z in the last convolutional layer of the network. Then, the global average pooling of the gradients (a_k^c) is used to show the importance weights for unit k .

$$a_k^c = \frac{1}{Z} \sum_x \sum_y \sum_z \frac{\partial y(c)}{\partial A_{x,y,z}^k} \quad (8)$$

where Z is the number of voxels in the corresponding convolutional layer. Then, we combined the unit weights with

the activations, $A_{x,y,z}^k$, to get the heatmap of 3D gradient-weighted class activation mapping.

$$L_{3D-Grad-CAM}^c = ReLU \left(\sum_k a_k^c A_{x,y,z}^k \right) \quad (9)$$

IV. EXPERIMENTAL EVALUATION

A. Dataset description

Data used in this study are from the ADNI (<http://adni.loni.usc.edu>), consisting of baseline MRI scans of 1407 subjects from ADNI-1, ADNI-2 and ADNI-3 datasets. These subjects are divided into three classes: AD (Alzheimer’s disease), MCI (mild cognitive impairment) and NC (normal control) based on the standard clinic criteria (e.g., Mini-Mental State Examination (MMSE) scores and Clinical Dementia Rating (CDR)). For MCI conversion prediction, MCI subjects are further divided into two classes: pMCI (progressive MCI subjects who had converted to AD within 36 months after baseline visit) and sMCI (stable MCI subjects who were continuously diagnosed as MCI). The ADNI-1 consists of 1.5T T1-weighted MR images, which has 835 scans of four classes: 200 of Alzheimer’s Disease (AD) patients and 231 of Normal Cohort (NC), 232 sMCI and 172 pMCI. The ADNI-2 dataset consists of 3T T1-weighted MR images, which contains 258 scans of four classes: 108 of AD patients and 150 of NC. The ADNI-3 dataset consists of 3T T1-weighted MR images similar to ADNI-2, which has 314 scans of four classes: 45 of AD patients and 269 of NC. The demographic information of subjects is presented in Table I.

In this work, we have used ADNI-1 for our model construction. ADNI-2 and ADNI-3 dataset have been used for independent cross-validation of model generalizability.

TABLE I
DEMOGRAPHIC INFORMATION IN THE USED DATASET. GENDER REPORTS ARE MALE AND FEMALE. THE AGE, EDUCATION YEARS, AND MINI-MENTAL STATE EXAMINATION (MMSE) VALUES ARE REPORTED.

Dataset	Group	Gender	Age	Edu	MMSE
		(Male/Female)	(Mean ± Std)	(Mean ± Std)	(Mean ± Std)
ADNI-1	AD	200 (103 / 97)	75.62 ± 7.70	14.68 ± 3.20	23.29 ± 2.04
	pMCI	172 (106 / 66)	76.34 ± 7.15	15.76 ± 2.84	26.61 ± 1.70
	sMCI	232 (154 / 78)	76.47 ± 7.82	15.58 ± 3.17	27.31 ± 1.79
	NC	231 (119 / 112)	75.99 ± 5.00	16.06 ± 2.84	29.12 ± 0.99
ADNI-2	AD	108 (60 / 48)	74.95 ± 7.80	15.88 ± 2.66	23.03 ± 2.14
	NC	150 (73 / 77)	74.84 ± 6.60	16.63 ± 2.48	29.09 ± 1.19
ADNI-3	AD	45 (25 / 20)	74.87 ± 8.701	15.98 ± 2.22	22.76 ± 3.58
	NC	269 (97 / 172)	70.72 ± 6.50	16.80 ± 2.25	29.09 ± 1.11

As the original dataset is in Neuroimaging Informatics Technology Initiative (NIfTI) format, the preprocessing is needed for spatial distortion correction caused by gradient nonlinearity and B1 field inhomogeneity. This is a standard pipeline process including anterior commissure (AC)-posterior commissure (PC) correction, intensity correction [53] and skull stripping [54]. We have used MIPAV (Medical Image Processing, Analysis, and Visualization) application to complete AC-PC correction and use FSL (FMRIB Software Library v6.0) to complete skull stripping. A line align registration strategy (flirt instruction in FSL) is also executed to align every sMRI linearly with the Colin27 template [55] to delete global linear differences (including global translation, scale, and rotation differences), and also to re-sample all sMRIs to have identical spatial resolution.

B. Evaluation metrics

We have evaluated two binary classification tasks of AD classification (i.e., AD vs. NC) and MCI conversion prediction (i.e., pMCI vs. sMCI). The classification performance has been evaluated based on four commonly used standard metrics, including classification accuracy (ACC), sensitivity (SEN), specificity (SPE), and Area under the curve (AUC). These metrics are defined as:

$$ACC = \frac{TP + TN}{TP + TN + FP + FN} \quad (10)$$

$$SEN = \frac{TP}{TP + FN} \quad (11)$$

$$SPE = \frac{TN}{TN + FP} \quad (12)$$

where $TP = TruePositive$, $TN = TrueNegative$, $FP = FalsePositive$ and $FN = FalseNegative$. The AUC is calculated based on all possible pairs of SEN and $1 - SPE$ obtained by changing the thresholds performed on the classification scores yielded by the trained networks.

C. Experimental evaluation

To evaluate performance and generalizability of our proposed model, we have conducted three types of experiments: 1) Comparison study with state-of-the-art 3D convolutional neural networks; 2) Evaluation on generalizability of the proposed model using two independent datasets (ADNI-2 and ADNI-3); 3) Comparison study with other existing machine learning/deep learning methods for AD diagnosis.

1) Evaluation 1: Comparison study with state-of-the-art 3D convolutional neural networks:

We have performed comparison study with most commonly used 3D convolutional neural networks including 3D-VGGNet, 3D-ResNet under two conditions: with and without self-attention mechanism in 18 and 34 layers. The structures of 3D-VGG Block, 3D-ResNet Block and 3D-ResAttNet Block are shown in Fig. 2.

Each Conv3D layer consists of 3 consistent operations: 3D convolution, batch normalization 3D and RELU. The 14 layers and 34 layers network contain 8 and 14 3D Resnet block and 3D-ResAttNet block, respectively. A $3 \times 3 \times 3$ 3D convolution is 3 times more expensive than 2D version in terms of computational cost. In order to reduce the computational cost, we have replaced the $7 \times 7 \times 7$ convolution in the 3D Conv block with three conservative $3 \times 3 \times 3$ convolutions. The detailed configuration is shown in Fig. 3.

In this evaluation, we have trained our model using ADNI-1 dataset and performed a 5 fold cross-validation. The dataset is randomly split into 5 groups where 4 groups (80% of the dataset) are used for training and the rest are used for testing each time. The experimental results for classification performance are the average of the accuracies on the testing set across all folds, along with Standard deviation (Std). p-value are also used to evaluate the statistical significance. To optimize model parameters, Adam, a stochastic optimization algorithm, with a batch size of 8 samples, has been used for optimization to train the proposed network [56]. We firstly

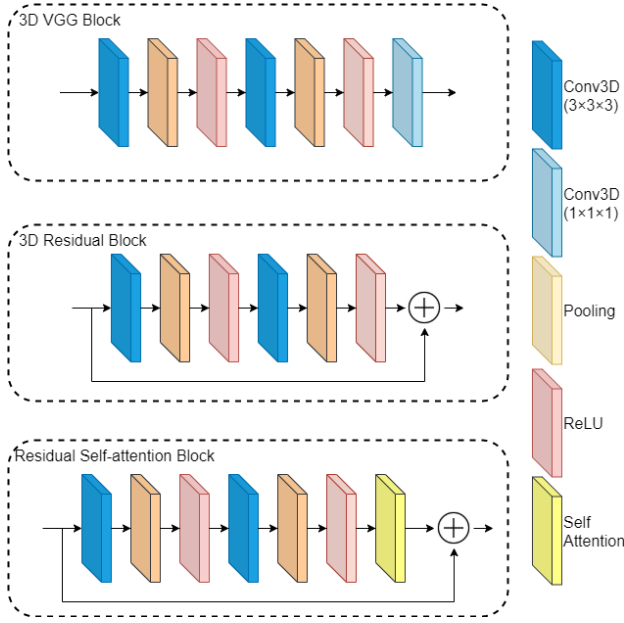


Fig. 2. The structure of 3D-VGG Block, 3D-ResNet Block and 3D-ResAttNet Block.

Layer name	Output size	3D-VGGNet	3D-ResNet18	3D-ResAttNet18	3D-ResNet34	3D-ResAttNet34
Input	181x171x181					
Input stem	91x109x91			Pooling layer (3x3x3) (3x3x3)		
Conv1	46x55x46	(3x3x3) (3x3x3)	(3x3x3) x 2 (3x3x3) x 2	(3x3x3) x 2 (3x3x3) x 2 Attention/	(3x3x3) x 3 (3x3x3) x 3	(3x3x3) x 3 (3x3x3) x 3 Attention/
Conv2	23x28x23	(3x3x3) (3x3x3) (1x1x1)	(3x3x3) x 2 (3x3x3) x 2	(3x3x3) x 2 (3x3x3) x 2 Attention/	(3x3x3) x 4 (3x3x3) x 4	(3x3x3) x 4 (3x3x3) x 4 Attention/
Conv3	12x14x12	(3x3x3) (3x3x3) (1x1x1)	(3x3x3) x 2 (3x3x3) x 2	(3x3x3) x 2 (3x3x3) x 2 Attention/	(3x3x3) x 6 (3x3x3) x 6	(3x3x3) x 6 (3x3x3) x 6 Attention/
Conv4	6x7x6	(3x3x3) (3x3x3) (1x1x1)	(3x3x3) x 2 (3x3x3) x 2	(3x3x3) x 2 (3x3x3) x 2 Attention/	(3x3x3) x 3 (3x3x3) x 3	(3x3x3) x 3 (3x3x3) x 3 Attention/
Pooling			Max Pooling			
Total trainable parameters		13,673,172	33,817,992	33,822,088	64,127,624	64,133,720

Fig. 3. Overall architecture of 3D CNNs models, including 3D-VGGNet, 3D-ResNet 18, 3D-ResAttNet 18, , 3D-ResNet 34 and , 3D-ResAttNet 34.

set the learning rate (LR) as 1×10^{-4} . The LR is decreased to 1×10^{-6} with increased iterations. CrossEntropy has been selected as the loss function for this task [57]).

All the experiments have been implemented based on Py-Torch and executed on a server with an Intel(R) Xeon(R) CPU E5-2650, NVIDIA 2080TI and 64 GB memory.

2) Evaluation 2: Evaluation on generalizability of the proposed model using two independent datasets:

To investigate generalizability and reproducibility of our proposed model, we have conducted two groups of experimental evaluation as follows:

- We have first built our model based on ADNI-1 and evaluated it using two independent datasets (ADNI-2 and ADNI-3 respectively).
- Then we reversed the training and testing datasets where we have trained the model using ADNI-2, and evaluated it on ADNI-1 and ADNI3 respectively.

In this evaluation, we only performed AD vs. NC classification task due to insufficient pMCI and sMCI samples obtained from ADNI-2 and ADNI-3.

3) Evaluation 3: Comparison study with other existing machine learning/deep learning methods for AD diagnosis:

For indirect evaluation, we have selected most recent and state-of-the-art machine learning methods reported in the literature for indirect comparison using baseline sMRI data from ADNI [10], [29], [15], [58], [59], [60], [61].

D. Result and discussion

1) Results from evaluation 1:

As introduced previously, we have added the attention mechanism in the Resnet block. In this group of experiments, we have compared the models including 3D-VGGNet and 3D-ResNet models with and without attention layer. The results are presented in Table II. The classification performance of models with attention layer are significantly higher than models without it, especially on pMCI vs. sMCI classification. Our proposed model (3D-ResAttNet34) shows the best performance in all experiments. Fig. 4 shows the examples of classification results for two classification tasks: AD vs. NC and pMCI vs. sMCI tasks. Fig. 4 a) shows an example on AD vs. NC classification where the classification result using our proposed model 3D-ResAttNet34 with attention layer classifies the image into a normal category (i.e. NC) while the result from 3D-ResNet34 classifies the image into disease category (i.e. AD). Similarly, Fig. 4 b) shows an example on pMCI vs. sMCI classification. It indicates that our model correctly identifies the images into the right categories.

TABLE II
RESULTS OF CLASSIFICATION FOR AD VS. NC AND pMCI VS. sMCI

Model	AD vs. NC classification			
	ACC \pm Std	SEN \pm Std	SPE \pm Std	AUC \pm Std
3D-VGGNet	0.807 \pm 0.046	0.798 \pm 0.049	0.829 \pm 0.036	0.890 \pm 0.036
3D-ResNet18	0.851 \pm 0.102	0.849 \pm 0.103	0.855 \pm 0.102	0.920 \pm 0.076
3D-ResAttNet18	0.860 \pm 0.088	0.829 \pm 0.119	0.903 \pm 0.052	0.975 \pm 0.023
3D-ResNet34	0.882 \pm 0.147	0.890 \pm 0.141	0.883 \pm 0.148	0.929 \pm 0.089
3D-ResAttNet34	0.913 \pm 0.012	0.910 \pm 0.014	0.919 \pm 0.009	0.984 \pm 0.009
Model	pMCI vs. sMCI classification			
	ACC \pm Std	SEN \pm Std	SPE \pm Std	AUC \pm Std
3D-VGGNet	0.758 \pm 0.059	0.751 \pm 0.083	0.735 \pm 0.060	0.856 \pm 0.056
3D-ResNet18	0.777 \pm 0.079	0.775 \pm 0.092	0.753 \pm 0.075	0.890 \pm 0.034
3D-ResAttNet18	0.799 \pm 0.071	0.810 \pm 0.093	0.775 \pm 0.071	0.926 \pm 0.053
3D-ResNet34	0.807 \pm 0.047	0.826 \pm 0.054	0.798 \pm 0.055	0.954 \pm 0.033
3D-ResAttNet34	0.821 \pm 0.092	0.812 \pm 0.101	0.809 \pm 0.097	0.920 \pm 0.047

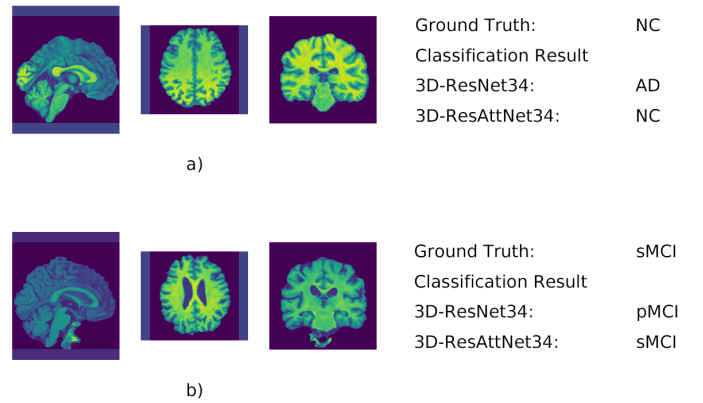


Fig. 4. Examples of classification results on a) the AD vs. ND classification task. The result shows the proposed method classified the image into the right category same as the ground truth (NC) while 3D ResNet34 classified into a wrong category (AD); b) the sMCI VS. pMCI task. The result shows the proposed method classified it into the right category same as the ground truth while 3D ResNet34 classified into a wrong category (pMCI)

For the explainable model evaluation, 3D Grad-CAM has been used to explain the model for Alzheimer’s Disease Diagnosis. We have only applied the 3D Grad-CAM to 3D-ResAttNet34 with the best classification performance. The heat-map is created to show how the network learns the importance of the areas. As described earlier, the 3D Grad-CAM can be used on an arbitrary layer. Fig. 5 shows feature visualizations of each convolution block from our proposed model (the top 64 activation maps are selected here). As more convolutions are processed, the resolution of the feature map also gradually decreases. In the first two convolution layers, the results have higher resolutions, which provide more details information. However, because they respond more to the corners, edge, texture and color conjunctions, more edges are highlighted. In the third and fourth convolution layers, the feature maps look like binary patterns where global and semantic information can be extracted. Some significant variation in lateral ventricle and hippocampus areas are highlighted.

The attention heatmap of the Grad-CAM on 3D-ResAttNet34 result is presented in Fig. 6. For comparison, the hippocampus, lateral ventricle and cerebral cortex areas on the input sMRI image in the first row are labeled to show the important areas for Alzheimers disease diagnosis. In the second row, we have applied the activation mapping heat-map to the last convolutional layer (i.e the fourth layer in this case). The heatmap is blurry because the last convolutional layer of 3D-ResAttNet34 is only of size $6 \times 7 \times 6$. The heat map tends to show global information. To obtain a higher resolution and more detailed 3D class activation mapping heat-map, we have applied the 3D Grad-CAM to the lower convolutional layer (the third layer), as shown in the third row of Fig. 6. It is of size $46 \times 55 \times 46$ heat-map and thus provides more detail information. It identifies and highlights the hippocampus, lateral ventricle and most parts of the cortex as important areas, which matches the human expert’s approach [24], [62]. However, as mentioned in [63], the lower layer in deep CNN models responds more to corners and edge/color conjunctions. Therefore, edges are highlighted as well.

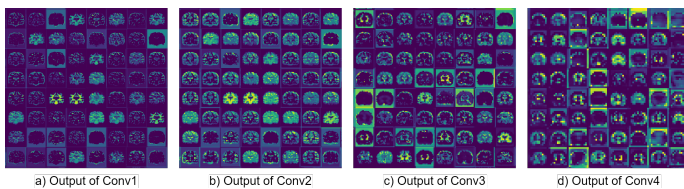


Fig. 5. Visualization results of selected convolutional layer feature maps. From left to right: first, second, third and fourth convolutional block.

2) Results for evaluation 2:

The evaluation result for generalizability of the proposed model are summarized in Table III.

For the first group of experiments, we have trained model using ADNI-1 dataset and evaluated it on ADNI-2 and ADNI-3 respectively. Comparing to our model based on ADNI-1 data, the accuracy on ADNI-2 is slightly decreased by 0.004 and the accuracy on ADNI-3 is slightly decreased by 0.021. The AUC is slightly dropped by 0.032 and 0.095 respectively. However, ACC, SEN, and SPE of our model remain high, which are

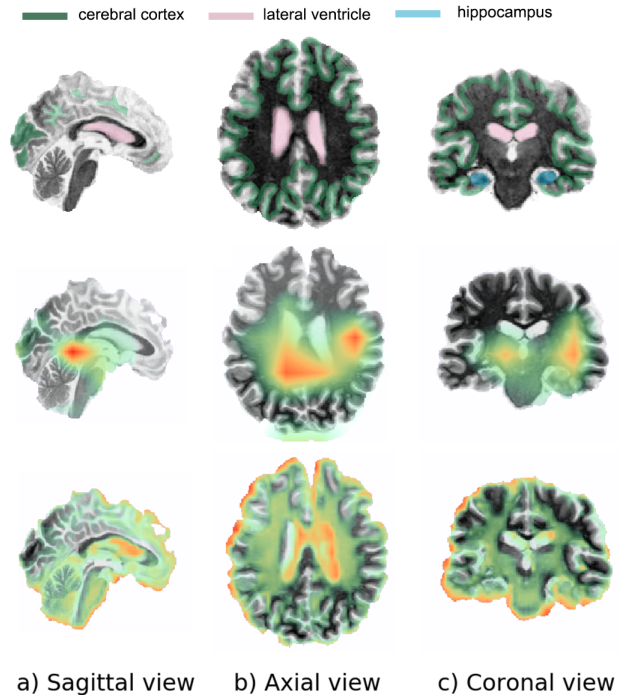


Fig. 6. Sagittal, Axial and coronal view of the brain MRI and the visual explanation heatmaps. The first row shows the highlighted cerebral cortex, lateral ventricle, and hippocampus areas in sMRI images. The second row shows the visualization by applying the Grad-Cam to the fourth convolutional layer. The third row shows the visualization by applying the Grad-Cam to the third layer.

statistically significant (i.e., p-values < 0.05). This shows the good generalizability of our proposed model.

For the second group of experiments, we have reversed the training and testing datasets to train the model using ADNI-2 and evaluate it on ADNI-1 and ADNI-3 respectively. The accuracy of our proposed model on ADNI-2 reaches 0.956. When testing on ADNI-1 and ADNI-3, the accuracies are 0.933 and 0.917 respectively, with slight decreases by 0.23 on ADNI-1 and 0.39 on ADNI-3 respectively. The ACC, SEN, and SPE of our proposed model based on ADNI-2 are higher than the ones of the model using ADNI-1, which are statistically significant (i.e., p-values < 0.05). The main reason is because ADNI-1 and ADNI-2 dataset are captured from distinct phases of the ADNI project, which have different signal to noise ratios (SNR). sMRI images from ADNI-1 are scanned using 1.5T scanners, while MR images from ADNI-2 are scanned using 3T scanners. The 3T scanner has twice sensitive compared to 1.5T which can generate clearer and higher quality image.

Based on these experiments, it has demonstrated that our proposed approach has good generalizability and reproducibility for AD diagnosis.

3) Results for evaluation 3:

It is unfair to perform the direct comparison between different methods due to the use of different datasets and also the clinical definition of pMCI/sMCI. In this case, we have only indirectly compared our model with six state-of-the-art machine learning based methods [64], [30], [65], [66], [67], [26].

TABLE III
THE MODEL PERFORMANCE ON INDEPENDENT DATASETS (ADNI-2 AND ADNI-3)

Model	Train	Evaluation	AD vs. NC classification			
			ACC \pm Std	SEN \pm Std	SPE \pm Std	AUC \pm Std
ADNI-1	ADNI-1	ADNI-1	0.913 \pm 0.012	0.910 \pm 0.014	0.919 \pm 0.009	0.984 \pm 0.009
	ADNI-1	ADNI-2	0.909 \pm 0.019	0.895 \pm 0.026	0.924 \pm 0.014	0.952 \pm 0.026
Proposed	ADNI-1	ADNI-3	0.892 \pm 0.034	0.788 \pm 0.060	0.780 \pm 0.076	0.889 \pm 0.034
	ADNI-2	ADNI-2	0.956 \pm 0.089	0.950 \pm 0.100	0.950 \pm 0.100	0.978 \pm 0.044
3D-ResAttNet34	ADNI-2	ADNI-1	0.933 \pm 0.133	0.933 \pm 0.133	0.930 \pm 0.140	0.967 \pm 0.067
	ADNI-2	ADNI-3	0.917 \pm 0.019	0.885 \pm 0.068	0.821 \pm 0.046	0.930 \pm 0.023

The results are shown in Table IV. There are several important observations including: 1) for the challenging task of MCI conversion prediction, the proposed 3D-ResAttNet outperforms other existing approaches; 2) for AD vs. NC classification, our proposed method has competitive performance, comparing to those methods using MRI only; 3) In terms of data size, our proposed method has been evaluated on a large number of subjects and cross-validated on two independent datasets from ADNI-2 and ADNI-3 respectively, which demonstrates a fair and independent evaluation and a good generalizability of our model. In addition, compared with the traditional region- and voxel-level pattern analysis methods, our proposed method takes the whole MRI image as input and automatically extracts high dimensional and nonlinear features, which leads to better classification performance for AD diagnosis.

TABLE IV
COMPARATIVE PERFORMANCE OF THE CLASSIFIER VS. SIX COMPETITORS ON ADNI DATASET.

References	Modality	Subject	Method	AD vs. NC classification			pMCI vs. sMCI classification		
				ACC	SEN	SPE	ACC	SEN	SPE
(Liu et al., 2014)	PET/MRI	65AD+169MCI+77NC	Stacked auto-encoder	0.88	0.89	0.87	0.77	0.74	0.78
(Suk et al., 2014)	PET/MRI	93AD+204MCI+101NC	Deep Boltzmann machine	0.95	0.95	0.95	0.76	0.48	0.95
(Aderghal et al., 2017a)	MRI	188AD+399MCI+228NC	2D-CNN	0.91	0.94	0.89	0.66	0.66	0.65
(Liu et al., 2018)	MRI	199AD+393MCI+229NC	Landmark detection + 3D CNN	0.91	0.88	0.94	0.77	0.42	0.82
(Shi et al., 2018)	MRI	41AD+99MCI+52NC	Deep polynomial network	0.95	0.94	0.96	0.75	0.63	0.85
(Lian et al., 2018)	MRI	358AD+670MCI+429NC	Hierarchical-CNN	0.90	0.82	0.97	0.81	0.53	0.85
Our 3D-ResAttNet on ADNI-1	MRI	200AD+404MCI+231NC	3D-CNN	0.91	0.91	0.92	0.82	0.81	0.81

V. CONCLUSION

Inspired by the attention mechanism and residual learning, we have proposed an end-to-end framework based on 3D Residual Self-Attention Network (3D ResAttNet) for early efficient diagnosis of AD diseases at two levels (i.e., AD vs. NC and pMCI vs. sMCI) from sMRI scans. The proposed method combines residual learning with self-attention mechanism, which can fully exploit both global and local information and avoid the information loss. Meanwhile, to understand inside our model and how our model reach decisions, we have also applied the 3D Grad-CAM method to identify and visualize those important areas contributing to our model decisions. To evaluate our model performance, we have compared the proposed model with most commonly used 3D convolutional neural networks including 3D-VGGNet, 3D-ResNet. The results show that our proposed model with attention layer (3D ResAttNet) outperforms the existing models. To evaluate generalization of the proposed model, we have also conducted thorough experiments under different cross-validation strategies using ADNI datasets (ADNI-1, ADNI-2 and ADNI-3): 1) building the proposed model based on ADNI-1 and then validating it on ADNI-2 and ADNI-3 respectively; 2) building the model based on ADNI-2 and then validating

it on ADNI-1 and ADNI-3 respectively. The results show that our proposed model has a good generalizability in all cases. Moreover, the explainable mechanism in our approach is able to identify and highlight the contribution of the important brain parts (e.g., hippocampus, lateral ventricle and most parts of the cortex) for transparent decisions. The future work will focus on continuous improvement of model performance and generalizability using more independent datasets.

ACKNOWLEDGMENT

The work reported in this paper has formed part of the project by Royal Society - Academy of Medical Sciences Newton Advanced Fellowship (NAF\R1\180371).

REFERENCES

- [1] WHO. Dementia. [Online]. Available: <https://www.who.int/news-room/fact-sheets/detail/dementia/>
- [2] O. B. Ahmed, M. Mizotin, J. Benois-Pineau, M. Allard, G. Catheline, C. B. Amar, and A. D. N. Initiative, "Alzheimer's disease diagnosis on structural MR images using circular harmonic functions descriptors on hippocampus and posterior cingulate cortex," *Computerized Medical Imaging and Graphics*, vol. 44, pp. 13–25, 2015.
- [3] C. Huang, L.-O. Wahlund, O. Almkvist, D. Elehu, L. Svensson, T. Jonsson, B. Winblad, and P. Julin, "Voxel- and VOI-based analysis of SPECT CBF in relation to clinical and psychological heterogeneity of mild cognitive impairment," *NeuroImage*, vol. 19, no. 3, pp. 1137–1144, Jul. 2003.
- [4] G. B. Frisoni, N. C. Fox, C. R. Jack Jr, P. Scheltens, and P. M. Thompson, "The clinical use of structural MRI in Alzheimer disease," *Nature Reviews Neurology*, vol. 6, no. 2, p. 67, 2010.
- [5] S. Rathore, M. Habes, M. A. Iftikhar, A. Shacklett, and C. Davatzikos, "A review on neuroimaging-based classification studies and associated feature extraction methods for Alzheimer's disease and its prodromal stages," *NeuroImage*, vol. 155, pp. 530–548, Jul. 2017. [Online]. Available: <http://www.sciencedirect.com/science/article/pii/S1053811917302823>
- [6] H. Alloui, M. Sadgal, and A. Elfaziki, "Utilization of a convolutional method for Alzheimer disease diagnosis," *Machine Vision and Applications*, vol. 31, no. 4, p. 25, May 2020. [Online]. Available: <http://link.springer.com/10.1007/s00138-020-01074-5>
- [7] E. Hosseini-Asl, G. Gimel'farb, and A. El-Baz, "Alzheimer's disease diagnostics by a deeply supervised adaptable 3D convolutional network," *arXiv preprint arXiv:1607.00556*, 2016.
- [8] A. Payan and G. Montana, "Predicting Alzheimer's disease: a neuroimaging study with 3D convolutional neural networks," *arXiv preprint arXiv:1502.02506*, 2015.
- [9] T. D. Vu, H.-J. Yang, V. Q. Nguyen, A.-R. Oh, and M.-S. Kim, "Multimodal learning using convolution neural network and Sparse Autoencoder," in *2017 IEEE International Conference on Big Data and Smart Computing (BigComp)*. IEEE, 2017, pp. 309–312.
- [10] J. C. Baron, G. Chetelat, B. Desgranges, G. Perchev, B. Landeau, V. De La Sayette, and F. Eustache, "In vivo mapping of gray matter loss with voxel-based morphometry in mild Alzheimer's disease," *Neuroimage*, vol. 14, no. 2, pp. 298–309, 2001.
- [11] J. Ashburner and K. J. Friston, "Why voxel-based morphometry should be used," *Neuroimage*, vol. 14, no. 6, pp. 1238–1243, 2001.
- [12] J. Ashburner and K. J., "Voxel-based morphometry: the methods," *Neuroimage*, vol. 11, no. 6, pp. 805–821, 2000.
- [13] A. Mechelli, C. J. Price, K. J. Friston, and J. Ashburner, "Voxel-based morphometry of the human brain: methods and applications," *Current medical imaging reviews*, vol. 1, no. 2, pp. 105–113, 2005.
- [14] C. Studholme, C. Drapaca, B. Iordanova, and V. Cardenas, "Deformation-based mapping of volume change from serial brain MRI in the presence of local tissue contrast change," *IEEE transactions on Medical Imaging*, vol. 25, no. 5, pp. 626–639, 2006.
- [15] S. Klppel, C. M. Stonnington, C. Chu, B. Draganski, R. I. Scahill, J. D. Rohrer, N. C. Fox, C. R. Jack, J. Ashburner, and R. S. J. Frackowiak, "Automatic classification of MR scans in Alzheimers disease," *Brain : a journal of neurology*, vol. 131, no. Pt 3, pp. 681–689, Mar. 2008. [Online]. Available: <https://www.ncbi.nlm.nih.gov/pmc/articles/PMC2579744/>

- [16] O. B. Ahmed, J. Benois-Pineau, M. Allard, C. B. Amar, G. Catheline, and A. D. N. Initiative, "Classification of Alzheimers disease subjects from MRI using hippocampal visual features," *Multimedia Tools and Applications*, vol. 74, no. 4, pp. 1249–1266, 2015.
- [17] B. Magnin, L. Mesrob, S. Kinkinghuh, M. Plgrini-Issac, O. Colliot, M. Sarazin, B. Dubois, S. Lehricy, and H. Benali, "Support vector machine-based classification of Alzheimers disease from whole-brain anatomical MRI," *Neuroradiology*, vol. 51, no. 2, pp. 73–83, 2009.
- [18] E. Gerardin, G. Chtelat, M. Chupin, R. Cuingnet, B. Desgranges, H.-S. Kim, M. Niethammer, B. Dubois, S. Lehricy, and L. Garnero, "Multidimensional classification of hippocampal shape features discriminates Alzheimer's disease and mild cognitive impairment from normal aging," *Neuroimage*, vol. 47, no. 4, pp. 1476–1486, 2009.
- [19] B. Gutman, Y. Wang, J. Morra, A. W. Toga, and P. M. Thompson, "Disease classification with hippocampal shape invariants," *Hippocampus*, vol. 19, no. 6, pp. 572–578, 2009.
- [20] V. Planche, A. Ruet, P. Coup, D. Lamargue-Hamel, M. Deloire, B. Pereira, J. V. Manjon, F. Munsch, N. Moscufo, and D. S. Meier, "Hippocampal microstructural damage correlates with memory impairment in clinically isolated syndrome suggestive of multiple sclerosis," *Multiple Sclerosis Journal*, vol. 23, no. 9, pp. 1214–1224, 2017.
- [21] D. Zhang, Y. Wang, L. Zhou, H. Yuan, D. Shen, and A. D. N. Initiative, "Multimodal classification of Alzheimer's disease and mild cognitive impairment," *Neuroimage*, vol. 55, no. 3, pp. 856–867, 2011.
- [22] K. He, X. Zhang, S. Ren, and J. Sun, "Deep residual learning for image recognition," in *Proceedings of the IEEE conference on computer vision and pattern recognition*, 2016, pp. 770–778.
- [23] Y. LeCun, Y. Bengio, and G. Hinton, "Deep learning," *nature*, vol. 521, no. 7553, pp. 436–444, 2015.
- [24] Y. Mu and F. H. Gage, "Adult hippocampal neurogenesis and its role in Alzheimer's disease," *Molecular Neurodegeneration*, vol. 6, p. 85, Dec. 2011.
- [25] C. D. Billones, O. J. L. D. Demetria, D. E. D. Hostallero, and P. C. Naval, "Demnet: A convolutional neural network for the detection of Alzheimer's Disease and Mild Cognitive Impairment," in *2016 IEEE Region 10 Conference (TENCON)*. IEEE, 2016, pp. 3724–3727.
- [26] C. Lian, M. Liu, J. Zhang, and D. Shen, "Hierarchical Fully Convolutional Network for Joint Atrophy Localization and Alzheimer's Disease Diagnosis using Structural MRI," *IEEE Transactions on Pattern Analysis and Machine Intelligence*, pp. 1–1, 2018. [Online]. Available: <https://ieeexplore.ieee.org/document/8585141/>
- [27] C. Hinrichs, V. Singh, L. Mukherjee, G. Xu, M. K. Chung, S. C. Johnson, A. D. N. Initiative *et al.*, "Spatially augmented lppboosting for ad classification with evaluations on the adni dataset," *Neuroimage*, vol. 48, no. 1, pp. 138–149, 2009.
- [28] H. Bay, T. Tuytelaars, and L. Van Gool, "Surf: Speeded up robust features," in *European conference on computer vision*. Springer, 2006, pp. 404–417.
- [29] Y. Fan, D. Shen, R. C. Gur, R. E. Gur, and C. Davatzikos, "COMPARE: classification of morphological patterns using adaptive regional elements," *IEEE transactions on medical imaging*, vol. 26, no. 1, pp. 93–105, 2006.
- [30] H.-I. Suk, S.-W. Lee, and D. Shen, "Hierarchical Feature Representation and Multimodal Fusion with Deep Learning for AD/MCI Diagnosis," *NeuroImage*, vol. 101, pp. 569–582, Nov. 2014. [Online]. Available: <https://www.ncbi.nlm.nih.gov/pmc/articles/PMC4165842/>
- [31] A. Krizhevsky, I. Sutskever, and G. E. Hinton, "Imagenet classification with deep convolutional neural networks," in *Advances in neural information processing systems*, 2012, pp. 1097–1105.
- [32] K. Simonyan and A. Zisserman, "Very deep convolutional networks for large-scale image recognition," *arXiv preprint arXiv:1409.1556*, 2014.
- [33] H. Li, M. Habes, and Y. Fan, "Deep ordinal ranking for multi-category diagnosis of alzheimer's disease using hippocampal MRI data," *arXiv preprint arXiv:1709.01599*, 2017.
- [34] I. Sample, "Computer says no: why making ais fair, accountable and transparent is crucial," *The Guardian*, vol. 5, pp. 1–15, 2017.
- [35] J. Adebayo, J. Gilmer, I. Goodfellow, and B. Kim, "Local explanation methods for deep neural networks lack sensitivity to parameter values," *arXiv preprint arXiv:1810.03307*, 2018.
- [36] M. Alber, S. Lapuschkin, P. Seeger, M. Hägele, K. T. Schütt, G. Montavon, W. Samek, K.-R. Müller, S. Dähne, and P.-J. Kindermans, "investigate neural networks," *Journal of Machine Learning Research*, vol. 20, no. 93, pp. 1–8, 2019.
- [37] M. Bojarski, A. Choromanska, K. Choromanski, B. Firner, L. Jackel, U. Muller, and K. Zieba, "Visualbackprop: efficient visualization of cnns," *arXiv preprint arXiv:1611.05418*, 2016.
- [38] J. T. Springenberg, A. Dosovitskiy, T. Brox, and M. Riedmiller, "Striving for simplicity: The all convolutional net," *arXiv preprint arXiv:1412.6806*, 2014.
- [39] P.-J. Kindermans, K. T. Schütt, M. Alber, K.-R. Müller, D. Erhan, B. Kim, and S. Dähne, "Learning how to explain neural networks: Patternnet and patternattribution," *arXiv preprint arXiv:1705.05598*, 2017.
- [40] S. Bach, A. Binder, G. Montavon, F. Klauschen, K.-R. Müller, and W. Samek, "On pixel-wise explanations for non-linear classifier decisions by layer-wise relevance propagation," *PLoS one*, vol. 10, no. 7, 2015.
- [41] G. Montavon, S. Lapuschkin, A. Binder, W. Samek, and K.-R. Müller, "Explaining nonlinear classification decisions with deep taylor decomposition," *Pattern Recognition*, vol. 65, pp. 211–222, 2017.
- [42] B. Zhou, A. Khosla, A. Lapedriza, A. Oliva, and A. Torralba, "Learning deep features for discriminative localization," in *Proceedings of the IEEE conference on computer vision and pattern recognition*, 2016, pp. 2921–2929.
- [43] R. R. Selvaraju, M. Cogswell, A. Das, R. Vedantam, D. Parikh, and D. Batra, "Grad-cam: Visual explanations from deep networks via gradient-based localization," in *Proceedings of the IEEE international conference on computer vision*, 2017, pp. 618–626.
- [44] X. Zhang, Y. Wei, J. Feng, Y. Yang, and T. S. Huang, "Adversarial complementary learning for weakly supervised object localization," in *Proceedings of the IEEE Conference on Computer Vision and Pattern Recognition*, 2018, pp. 1325–1334.
- [45] H. Zhang, I. Goodfellow, D. Metaxas, and A. Odena, "Self-attention generative adversarial networks," *arXiv preprint arXiv:1805.08318*, 2018.
- [46] K. Li, Z. Wu, K.-C. Peng, J. Ernst, and Y. Fu, "Guided attention inference network," *IEEE transactions on pattern analysis and machine intelligence*, 2019.
- [47] C. Yang, A. Rangarajan, and S. Ranka, "Visual Explanations From Deep 3D Convolutional Neural Networks for Alzheimer's Disease Classification," *arXiv:1803.02544 [cs, stat]*, Jul. 2018, arXiv: 1803.02544. [Online]. Available: <http://arxiv.org/abs/1803.02544>
- [48] F. Wang, M. Jiang, C. Qian, S. Yang, C. Li, H. Zhang, X. Wang, and X. Tang, "Residual Attention Network for Image Classification," *arXiv:1704.06904 [cs]*, Apr. 2017, arXiv: 1704.06904. [Online]. Available: <http://arxiv.org/abs/1704.06904>
- [49] A. Vaswani, N. Shazeer, N. Parmar, J. Uszkoreit, L. Jones, A. N. Gomez, Ł. Kaiser, and I. Polosukhin, "Attention is all you need," in *Advances in neural information processing systems*, 2017, pp. 5998–6008.
- [50] X. Zhang, Y. Wei, G. Kang, Y. Yang, and T. Huang, "Self-produced guidance for weakly-supervised object localization," in *Proceedings of the European Conference on Computer Vision (ECCV)*, 2018, pp. 597–613.
- [51] X. Wang, R. Girshick, A. Gupta, and K. He, "Non-local neural networks," in *Proceedings of the IEEE conference on computer vision and pattern recognition*, 2018, pp. 7794–7803.
- [52] A. Buades, B. Coll, and J.-M. Morel, "A non-local algorithm for image denoising," in *2005 IEEE Computer Society Conference on Computer Vision and Pattern Recognition (CVPR'05)*, vol. 2. IEEE, 2005, pp. 60–65.
- [53] J. G. Sled, A. P. Zijdenbos, and A. C. Evans, "A nonparametric method for automatic correction of intensity nonuniformity in MRI data," *IEEE transactions on medical imaging*, vol. 17, no. 1, pp. 87–97, Feb. 1998.
- [54] Y. Wang, J. Nie, P.-T. Yap, F. Shi, L. Guo, and D. Shen, "Robust Deformable-Surface-Based Skull-Stripping for Large-Scale Studies," in *Medical Image Computing and Computer-Assisted Intervention MICCAI 2011*, ser. Lecture Notes in Computer Science, G. Fichtinger, A. Martel, and T. Peters, Eds. Berlin, Heidelberg: Springer, 2011, pp. 635–642.
- [55] C. J. Holmes, R. Hoge, L. Collins, R. Woods, A. W. Toga, and A. C. Evans, "Enhancement of MR images using registration for signal averaging," *Journal of Computer Assisted Tomography*, vol. 22, no. 2, pp. 324–333, Apr. 1998.
- [56] D. P. Kingma and J. Ba, "Adam: A Method for Stochastic Optimization," *arXiv:1412.6980 [cs]*, Jan. 2017, arXiv: 1412.6980. [Online]. Available: <http://arxiv.org/abs/1412.6980>
- [57] P.-T. De Boer, D. P. Kroese, S. Mannor, and R. Y. Rubinstein, "A tutorial on the cross-entropy method," *Annals of operations research*, vol. 134, no. 1, pp. 19–67, 2005.
- [58] J. Koikkalainen, J. Lijnen, L. Thurfjell, D. Rueckert, G. Waldemar, and H. Soininen, "Multi-template tensor-based morphometry: Application to analysis of Alzheimer's disease," *NeuroImage*, vol. 56, no. 3, pp. 1134–1144, Jun. 2011. [Online]. Available: <https://www.ncbi.nlm.nih.gov/pmc/articles/PMC3554792/>

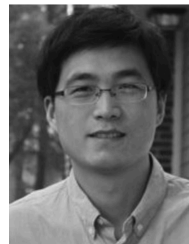
- [59] M. Liu, D. Zhang, and D. Shen, "Relationship Induced Multi-Template Learning for Diagnosis of Alzheimer's Disease and Mild Cognitive Impairment," *IEEE transactions on medical imaging*, vol. 35, no. 6, pp. 1463–1474, 2016.
- [60] C. Mller, Y. A. L. Pijnenburg, W. M. van der Flier, A. Versteeg, B. Tijms, J. C. de Munck, A. Hafkemeijer, S. A. R. B. Rombouts, J. van der Grond, J. van Swieten, E. Dopfer, P. Scheltens, F. Barkhof, H. Vrenken, and A. M. Wink, "Alzheimer Disease and Behavioral Variant Frontotemporal Dementia: Automatic Classification Based on Cortical Atrophy for Single-Subject Diagnosis," *Radiology*, vol. 279, no. 3, pp. 838–848, Jun. 2016.
- [61] C. Salvatore, A. Cerasa, P. Battista, M. C. Gilardi, A. Quattrone, I. Castiglioni, and Alzheimer's Disease Neuroimaging Initiative, "Magnetic resonance imaging biomarkers for the early diagnosis of Alzheimer's disease: a machine learning approach," *Frontiers in Neuroscience*, vol. 9, p. 307, 2015.
- [62] B. R. Ott, R. A. Cohen, A. Gongvatana, O. C. Okonkwo, C. E. Johanson, E. G. Stopa, J. E. Donahue, G. D. Silverberg, and Alzheimer's Disease Neuroimaging Initiative, "Brain ventricular volume and cerebrospinal fluid biomarkers of Alzheimer's disease," *Journal of Alzheimer's disease: JAD*, vol. 20, no. 2, pp. 647–657, 2010.
- [63] M. D. Zeiler and R. Fergus, "Visualizing and understanding convolutional networks," in *European conference on computer vision*. Springer, 2014, pp. 818–833.
- [64] S. Liu, S. Liu, W. Cai, S. Pujol, R. Kikinis, and D. Feng, "Early diagnosis of Alzheimer's disease with deep learning," in *2014 IEEE 11th International Symposium on Biomedical Imaging (ISBI)*, Apr. 2014, pp. 1015–1018, iSSN: 1945-8452.
- [65] K. Aderghal, M. Boissenin, J. Benois-Pineau, G. Catheline, and K. Afdel, "Classification of sMRI for AD Diagnosis with Convolutional Neuronal Networks: A Pilot 2-D+ ϵ Study on ADNI," in *MultiMedia Modeling*, ser. Lecture Notes in Computer Science, L. Amsaleg, G. . Gumundsson, C. Gurrin, B. . Jnsson, and S. Satoh, Eds. Cham: Springer International Publishing, 2017, pp. 690–701.
- [66] M. Liu, J. Zhang, E. Adeli, and D. Shen, "Landmark-based deep multi-instance learning for brain disease diagnosis," *Medical image analysis*, vol. 43, pp. 157–168, 2018.
- [67] J. Shi, X. Zheng, Y. Li, Q. Zhang, and S. Ying, "Multimodal Neuroimaging Feature Learning With Multimodal Stacked Deep Polynomial Networks for Diagnosis of Alzheimer's Disease," *IEEE journal of biomedical and health informatics*, vol. 22, no. 1, pp. 173–183, 2018.



Wenyong Zhu Wenyong Zhu received the B.S degree from Nanjing University of Aeronautics and Astronautics (NUAA), China, in 2019. And he is studying for a master's degree in NUAA. His current research interests include machine learning and medical image classification.



Sun Liang Liang Sun received the B.S degree from Shandong University of Science and Technology, China, in 2014, and Ph.D. degree in Computer Science and Technology from Nanjing University of Aeronautics and Astronautics (NUAA), China, in 2020. His current research interests include machine learning and medical image segmentation.



Daoqiang Zhang received the B.Sc. and Ph.D. degrees in computer science from Nanjing University of Aeronautics and Astronautics, Nanjing, China, in 1999 and 2004, respectively. He is currently a Professor in the Department of Computer Science and Engineering, Nanjing University of Aeronautics and Astronautics. His current research interests include machine learning, pattern recognition, and biomedical image analysis. In these areas, he has authored or coauthored more than 100 technical papers in the refereed international journals and conference proceedings.



Xin Zhang Xin Zhang is associate researcher in Manchester Metropolitan University (MMU), he received the B.S degree from The PLA Academy of Communication and Commanding, China, in 2009 and Ph.D. degree in Cartography and Geographic Information System from Beijing Normal University (BNU), China, in 2014. His current research interests include remote sensing image processing and deep learning.



Liangxiu Han received the Ph.D. degree in computer science from Fudan University, Shanghai, China, in 2002. She is currently a Professor of computer science with the School of Computing, Mathematics, and Digital Technology, Manchester Metropolitan University. Her research areas mainly lie in the development of novel big data analytics and development of novel intelligent architectures that facilitates big data analytics (e.g., parallel and distributed computing, Cloud/Service-oriented computing/data intensive computing) as well as applica-

tions in different domains using various large datasets (biomedical images, environmental sensor, network traffic data, web documents, etc.). She is currently a Principal Investigator or Co-PI on a number of research projects in the research areas mentioned above.